

Propulsion System Testing for a Long-Endurance Solar-Powered Unmanned Aircraft

Or D. Dantsker*

University of Illinois at Urbana–Champaign, Urbana, IL 61801

Robert W. Deters†

Embry-Riddle Aeronautical University - Worldwide, Daytona Beach, FL 32114

Marco Caccamo‡

Technical University of Munich (TUM), Garching, Germany

The increase in popularity of unmanned aerial vehicles (UAVs) has been driven by their use in civilian, education, government, and military applications. However, limited on-board energy storage significantly limits flight time and ultimately usability. The propulsion system plays a critical part in the overall energy consumption of the UAV; therefore, it is necessary to determine the most optimal combination of possible propulsion system components for a given mission profile, i.e. propellers, motors, and electronic speed controllers (ESC). Hundreds of options are available for the different components with little performance specifications available for most of them. In order to determine the performance specifications, a propulsion system testing apparatus has been developed and validated. This testing apparatus was designed to measure the performance and efficiency parameters of electric propulsion system components (propellers, motors, and ESC) while maintaining similar air flow characteristics in either a wind tunnel or on a moving automotive platform. Validation tests of four propellers are presented. All four propellers were tested under static conditions, and two were tested under advancing flow conditions where the testing apparatus was used on an automotive platform. The results show that this propulsion testing system provides for holistic testing of all possible compatible electric propulsion system components in a flight-like environment. Data from this system will be used in a mission-based propulsion system optimizer, currently in development, to select the best combination of components for a long-endurance solar-powered unmanned aircraft.

Nomenclature

AHRS	= attitude and heading reference system	i_s	= supply current
ESC	= electronic speed controller	i_0	= zero load motor current
GNSS	= global navigation satellite system	J	= advance ratio
IMU	= inertial measurement unit	K_v	= motor speed constant
PWM	= pulse width modulation	n	= propeller and motor rotation rate
RPM	= rotations per minute	p	= ambient pressure
UAV	= unmanned aerial vehicle	P_{elect}	= electrical power
		P_{motor}	= motor power
C_P	= power coefficient	P_{shaft}	= shaft power
C_T	= thrust coefficient	Q	= torque
D	= propeller diameter	R	= universal gas constant
i_m	= motor current	R_m	= internal motor resistance

*Ph.D. Student, Department of Aerospace Engineering, AIAA Student Member. dantskel@illinois.edu

†Assistant Professor, Department of Engineering and Technology, AIAA Member.

‡Professor, Department of Mechanical Engineering.

T	= thrust		
t	= ambient temperature	η_p	= propeller efficiency
V	= air flow velocity	η_m	= motor efficiency
V_{gps}	= GPS velocity	η_e	= electronic speed controller efficiency
U_m	= motor terminal voltage	ρ	= density of air
U_s	= supply voltage		

I. Introduction

In recent years, there has been an uptrend in the popularity of UAVs driven by the desire to apply these aircraft to areas such as precision farming, infrastructure and environment monitoring, surveillance, surveying and mapping, search and rescue missions, weather forecasting, and more. A key commonality across the aforementioned applications is the necessity of sensing. Notably, the majority of the aforementioned applications require continuous collection and processing of visual data (e.g. visible, IR, UV, and multi-spectral). The traditional approach for small size UAVs is to capture data on the aircraft, stream it to the ground through a high power data-link, process it remotely (potentially off-line), perform analysis, and then relay commands back to the aircraft as needed.¹⁻³ Since the inception of unmanned aircraft, a key design constraint has been energy storage as limited on-board energy storage significantly limits flight time and ultimately usability. Given the finite energy resources found onboard an aircraft (battery or fuel), traditional designs greatly limit aircraft endurance as significant power is required for propulsion, actuation, and the continuous transmission of visual data.

To truly enable a variety of applications, the overarching goal is to create a computationally-intensive, long-endurance solar-powered unmanned aircraft that would carry a high-performance embedded computer system to perform all required computations online and only downlink final results, saving a significant amount of energy. Currently, such an aircraft is in development: UIUC Solar Flyer,^{4,5} which is shown in Fig. 1. The completed 4.0 m (157 in) wingspan aircraft will weight approximately 2.5 kg (88 oz) and be instrumented with an integrated autopilot and high-fidelity data acquisition system with an integrated 3D graphics processing unit. Given the objective, to operate continuously during all-daylight hours, the aircraft will be powered by solar array, specifically gallium arsenide (GaAs) solar cells from Alta Devices, which hold the world record for solar efficiency and power density, will be used in conjunction with a maximum power point tracking (MPPT) charge controller and a small lithium polymer battery that will act as an energy buffer.

The critical choice in the UIUC Solar Flyer's development then becomes what type of propulsion system to use. A mission-based propulsion system optimizer is in development⁶ to select the most optimal combination of possible propulsion system components for a given mission profile, i.e. propellers, motors, and ESC. Currently, there are hundreds of propeller and dozens of motor and ESC options in the radio control model market for an airframe of this size, yielding thousands of possible choices. Therefore, the problem becomes gathering component parameters with often scarce performance specifications.



Figure 1: The baseline UIUC Solar Flyer aircraft shown without solar arrays.

This paper describes the development and validation of a propulsion system testing apparatus that is designed to evaluate potential components for a long-endurance solar-powered unmanned aircraft. Specifically, the testing apparatus, which is shown in Fig. 2, was developed to measure the performance and efficiency parameters of possible electric propulsion system components (propellers, motors, and ESC) while maintain similar air flow characteristic in either a wind tunnel or on a moving automotive platform. The propulsion system testing apparatus is instrumented with a high-frequency data acquisition system and sensors allowing for simultaneous load, torque, electrical, air data, and inertial measurement.

Previous works have measured the performance and efficiency parameters of electric UAV propulsion system components. Brandt^{7,8} and Uhlig^{9,10} explored the performance of low-Reynolds number propellers at slow speeds and past stall. Lundstrom performed a similar test using an automotive-based testing rig.^{11,12} Deters looked into the performance of micro propellers for both small/micro air vehicles,^{13,14} later expanding his work to look at static performance of micro propellers for quadrotors.^{15,16} Lindahl¹⁷ tested large UAV propellers in a wind tunnel while Chaney¹⁸ and Dantsker¹⁹ did so using automotive based rigs. Lindahl also tested the effects of using different motors with a given propeller. Drela has done extensive work testing and modelling motors and propellers.²⁰⁻²² Green²³ and Gong²⁴ have modelled and tested the efficiency of ESCs. Gong has also tested a propeller-motor combination in a wind tunnel²⁵ as well as create an in-flight thrust measurement system.²⁶ Compared to existing works in the literature, the propulsion system testing apparatus presented in this paper allows for holistic testing of all possible compatible electric propulsion system components in a flight-like environment. The energy supply source is not considered in this paper; however, the testing apparatus could easily be adapted to accommodate such testing.

This paper will first examine the requirements for the propulsion system testing apparatus. Then a description of the development will be given. This will be followed by a discussion of data reduction methodology. Next, an preliminary testing will be presented and discussed. Finally, a summary and statement of future work will be given.



Figure 2: A photo of the propulsion system testing apparatus with folding propeller and pitot-static probe.

II. Requirements

It was desired that the propulsion system testing apparatus be able to measure the performance and efficiency characteristics for a wide range of propellers, motors, and ESCs while being able to simulate the conditions these components would face in actual flight. Specifically, three key requirement areas of interest that drove the design were (1) operational similarity, (2) measurement capability, and (3) test component compatibility.

A. Operational Similarity

The propulsion system testing apparatus should be able to simulate the conditions which the propeller, motor, and ESC will experience in-flight on the solar-powered unmanned aircraft. Specifically, the main aspect of concern is that the air flow the propeller experiences will mimic what is exhibited in actual flight. As the motor and propeller are bound to the nose of the aircraft, the nose geometry of the aircraft will dictate the air flow patterns expected in the apparatus design. Likewise, the downstream geometry should be designed in such a way as to minimally effect the flow at the propeller location. Finally, the testing environment should provide clean, uniform flow as would be exhibited in flight. This flow requirement means that a wind tunnel should be sufficiently large such that there are minimal wall effects or that a moving automotive platform be far enough above the vehicle such that it is outside of the vehicle boundary layer.

B. Measurement Capabilities

In order to conduct a proper comparison between possible propulsion system components, the propulsion system testing apparatus must be capable of recording all relevant/required measurements. Based on previous work, the following measurement capabilities were identified as required for wind tunnel-based testing:

- motor-propeller thrust T , torque Q , and rotation rate n
- motor voltage U_m and current i_m
- supply voltage U_s and current i_s
- air flow velocity V , ambient pressure p , ambient temperature t

If the propulsion system testing apparatus is operated on an automotive platform, the following additional measurement capabilities are also required:

- GPS velocity V_{gps} and position
- inertia accelerations, rotation rates, and Euler angles

These measurements allow for the estimation of wind as well as the vibration and motion associated with the automotive platform.

It was also desired that the instrumentation be able to acquire the above fields at the highest realistic frequency possible. This requirement follows that noise can be averaged out more effectively as the acquisition rate increases. Based on the range of commercially available components (i.e. size, compatibility, price, and availability) as well as previous experience integrating data acquisition systems into aircraft (e.g. interfacing with ESC),^{4,19,27-30} a desired acquisition rate is in the order of 100 to 400 Hz, with preference towards to the higher end.

C. Test Component Compatibility

The propulsion system testing apparatus should be able to mount and provide support for all possible propulsion system components that could be used on the actual solar-powered unmanned aircraft: propellers, motors, and ESCs. Tables 1 and 2 list the propellers and motors, respectively, that were of interest to test. Aero-Naut CAM carbon propellers³¹ are well known in the UAV industry to offer superior performance and are ubiquitous;³²⁻³⁵ however, little performance data exists. Currently, a CAM 13×6.5 propeller is being used on the UIUC Solar Flyer, and based on recent testing, it is well oversized for the application.⁴ Therefore, testing a range of CAM propellers with diameters of 8 to 12.5 in is desired. Similarly, the motor currently being used on the Solar Flyer is also oversized and thus other motors are of interest to test; note that the desired motor testing not only confirms the motor parameters discussed in Section IV, but also verifies that the motor is able to operate continuously for long periods of time without overheating or wearing out. Currently, only the Castle Creations Phoenix Edge 50 Lite ESC is of interest to test, due to previous development and integration efforts of the UIUC Solar UAV. It should be noted that the use of this ESC is not meant to be a general requirement for the propulsion system testing apparatus but rather a need for the current application.

Table 1: Aero-Naut CAM Carbon Propellers of Interest for Testing

Aero-Naut Propellers						
CAM 8×5	CAM 9×4	CAM 9.5×5	CAM 10×4	CAM 11×6	CAM 12×5	CAM 12.5×6
CAM 8×6	CAM 9×5	CAM 9.5×6	CAM 10×5	CAM 11×7	CAM 12×6	CAM 12.5×7.7
CAM 8×7	CAM 9×6	CAM 9.5×7	CAM 10×6	CAM 11×8	CAM 12×6.5	CAM 12.5×9
	CAM 9×7		CAM 10×7	CAM 11×10	CAM 12×8	
			CAM 10×8	CAM 11×12	CAM 12×9	
			CAM 10×12		CAM 12×10	
					CAM 12×13	

Table 2: Motors of Interest for Testing

Model Motors ³⁶	Hacker Motors ³⁷	Neu Motors ³⁸
AXi Cyclone 550/720	A30-12L V2-6 Pole +6,7:1	1105/3.5Y w/4.4:1
AXi Cyclone 480/840	A30-18M V2-6 Pole +6,7:1	1105/3Y w/4.4:1
AXi 480 2220/20	A30-14M V2-6 Pole +6,7:1	
AXi 480 2217/20	A20-6XL V2-10 Pole +4,4:1	
AXi 400 2212/34	A20-8XL V2 +4,4:1	

III. Design and Development

The design and development of the propulsion system testing apparatus was split between several efforts: (1) inertial testing assembly (2) instrumentation, and (3) automotive platform mount.

A. Testing Assembly

The core module of the propulsion system testing apparatus is the testing assembly, which contains the load and torque cells and provides a mounting area for the motor and propeller. An isometric rendering and a side-view with covers removed are provided in Figs. 3 and 4, respectively. The testing assembly is composed of a nylon 3D-printed nose fairing, which transfers the thrust and torque from the motor and to the torque cell. The 3D-printed nose fairing duplicates the geometry of the forward section of the UIUC Solar Flyer fuselage. The torque cell is then connected to the load cell through an aluminum piece. Finally, the load cell is mounted to a square perforated steel tube through an aluminum insert. The square perforated steel tube can either be bolted to the floor of a wind tunnel or to an automobile via the automotive platform mount. All of the components behind the torque transducer were shrouded in airfoil shaped fairings to reduce the effects of the propeller slipstream on the torque and thrust measurements.

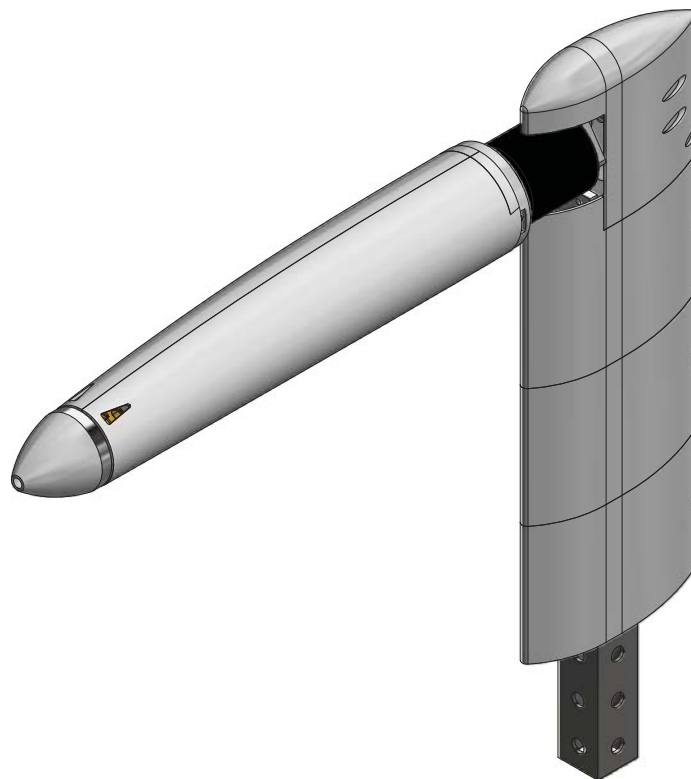


Figure 3: An isometric CAD rendering of the apparatus testing assembly.

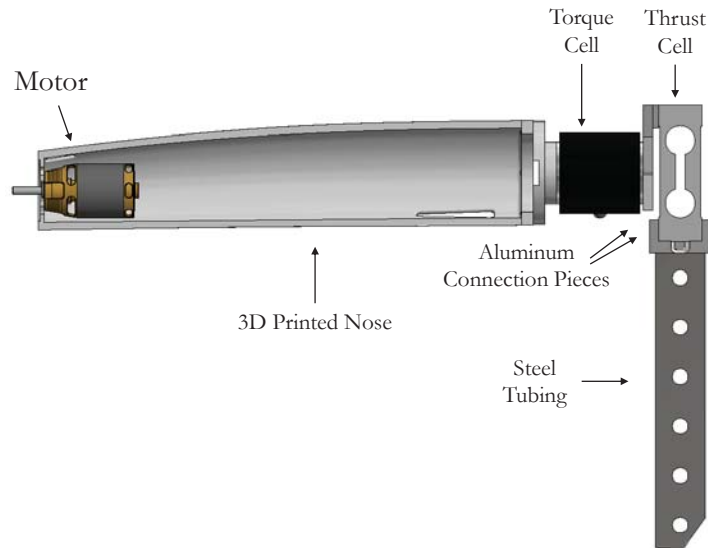


Figure 4: An annotated side-view CAD rendering of the propulsion system testing apparatus testing assembly with the rear fairings and half of the forward cover removed.

B. Instrumentation

The propulsion system testing apparatus was instrumented with a high-frequency data acquisition system as well as a variety of sensors. The testing assembly region of the apparatus contains a load cell and a torque cell, which measure the thrust and torque produced by the propeller during testing. The remainder of the sensors are located below the testing assembly region and include: an ESC data interface (which provides RPM and motor output voltage and current), a supply voltage and current measurement sensor, and an air data sensor.

A computer-controlled PWM signal driver is also present in the testing apparatus to command the ESC throttle. If the testing apparatus is mounted to a moving platform, a global navigation satellite system (GNSS) receiver, an inertial measurement unit (IMU), and a calibrated pitot-static probe will also be used. All of the instrumentation, less the load and torque cells, have previously been used and calibrated. The component specifications for the propulsion system testing apparatus instrumentation are provided in Table 3.

The instrumentation enables: inline measurement of thrust (T) and torque (Q) at the motor; ESC data collection of rotation rate (n), motor voltage (U_m), and motor current (i_m); upstream measurement of supply voltage (U_s) and current (i_s); air data measurement of flow speed (V_a), temperature (t), and pressure (p). If mounted to a moving platform, the system additionally measures global position and velocity (V_g) as well as platform orientation, rotation rates, and accelerations. These measurement capabilities enable the determination of propeller thrust coefficient (C_T), power coefficient (C_P), and efficiency (η_p) vs. advance ratio (J) curves; motor parameters including zero load current (i_0), internal resistance (R), speed constant (K_v), and motor efficiency (η_m); and ESC efficiency (η_e).

Table 3: Specifications of the Propulsion System Testing Apparatus

Data acquisition system	Al Volo FDAQ 400 Hz system ³⁹
Inertial and Flow Sensors	
Inertial	100 Hz IMU AHRS integrated into FC+DAQ
Positioning	10 Hz GNSS integrated into FC+DAQ
Airspeed Sensor	Al Volo Pitot Static Airspeed Sensor
ESC Sensor and Driver	
ESC Sensor Data Interface	Al Volo Castle ESC Interface
ESC PWM Driver	PIC18 based microcontroller
Power Sensors	
Voltmeter	Voltage divider circuit connected to FDAQ analog input
Ammeter	Allegro MicroSystems ACS758 DC hall-effect 50 A current sensor
Force/Torque Sensors	
Thrust Sensor	LSP-2 beam-type 2 kg load cell by Transducer Techniques ⁴⁰
Torque Sensor	RTS-100 reaction-type 100 oz-in torque sensor by Transducer Techniques
Wheatstone Bridge	Custom integration by Al Volo LLC

C. Automotive Platform Mount

The automotive platform mount was developed to adapt the propulsion system testing apparatus for car top testing. Essentially, the platform mount is a triangular frame that provides rigid support between the testing assembly and a standard automotive roof rack. The frame was constructed from aluminum and steel square tubing, angle, and bars, and can easily attach the testing assembly on top. The mount also provides a connection point for a pitot-static probe to be added. An isometric CAD rendering of the testing apparatus attached to the automotive platform mount is shown in Fig. 5.



Figure 5: An isometric CAD rendering of the propulsion system testing apparatus with the automotive platform mount and pitot-static probe.

IV. Data Reduction

Data produced by the propulsion system testing apparatus are used to calculate overall efficiency of the system for a given flight state. The thrust output power produced is equal to the product of the system input power and the component efficiencies: propeller efficiency, motor efficiency, and ESC efficiency. The relationship is summarized as follows:

$$P_{thrust} = \eta_p \cdot \eta_m \cdot \eta_e \cdot P_{input} \quad (1)$$

Individual efficiencies are now examined including how they are derived from data. It should be noted that the efficiencies depend on numerous factors that are directly or indirectly related to the components, the aircraft flight state, and the environment.

A. Propeller

From the thrust, torque, rotation rate, and flow velocity values, the thrust coefficient, power coefficient, and propeller efficiency values are calculated. In order to perform these calculations, knowledge of the air density and propeller diameter is required. Using the temperature and pressure readings, the air density is determined using the equation of state

$$p = \rho R t \quad (2)$$

where R is the universal gas constant with a value for air of $287.0 \text{ m}^2/\text{s}^2/\text{K}$ ($1716 \text{ ft}^2/\text{s}^2/\text{R}$).

The propeller advance ratio J is defined from the ratio of the measured air flow speed V to the propeller rotation rate n (in rev/s) and the propeller diameter D as

$$J = \frac{V}{nD} \quad (3)$$

The thrust coefficient C_T is calculated from the measured thrust T , rotation rate, air density, and the propeller diameter as

$$C_T = \frac{T}{\rho n^2 D^4} \quad (4)$$

In order to determine the power coefficient, propeller shaft output power P_{shaft} must be found. Propeller shaft power is determined from the measured torque Q and rotation rate by

$$P_{shaft} = 2\pi n Q \quad (5)$$

Therefore, the power coefficient C_P can be calculated from the measured rotation rate, propeller shaft power, air density, and the propeller diameter as

$$C_P = \frac{P_{shaft}}{\rho n^3 D^5} \quad (6)$$

Finally, the propeller efficiency η_p can be determined as

$$\eta_p = J \frac{C_T}{C_P} \quad (7)$$

B. Motor

From the torque, rotation rate, and power input into the motor, the motor efficiency η_m is calculated. The motor efficiency is defined as the ratio between the shaft output power P_{shaft} and the motor input power P_{motor} .

$$\eta_m = \frac{P_{shaft}}{P_{motor}} \quad (8)$$

The motor input power P_{motor} is calculated as the product of the motor terminal voltage U_m and motor current i_m , which are measured by the ESC.

$$P_{motor} = U_m i_m \quad (9)$$

The motor shaft output power is equal to the propeller shaft power given in Equation 5. Therefore the motor efficiency can be determined as

$$\eta_m = \frac{2\pi n Q}{U_m i_m} \quad (10)$$

Once the motor efficiency values are known, motor parameters can be computed. A first order approximation²¹ for the motor efficiency as a function of the motor terminal voltage and shaft rotation rate, and a variety of fixed motor parameters, is given as

$$\eta_m(\Omega, U_m) = \left(1 - \frac{i_0 R_m}{U_m - n/K_v}\right) \frac{n}{U_m K_v} \quad (11)$$

where i_0 as motor current at zero load, R as motor internal resistance and K_v as motor speed constant. Given a large enough sample size, these parameters can be fitted using regression or other means.

C. ESC

A variety of methods exist²³⁻²⁵ to calculate ESC efficiency, η_e . These generally yield that ESC efficiency is a function of voltage and current. Depending on the formulation, these relationships are inverse, linear, and/or quadratic and rely on many constants. Sometimes duty cycle, which is proportional to shaft rotation rate and can be proportional to throttle input, is also taken into account.

For the purposes of this paper, the ESC will be treated as a black box where efficiency is calculated as the ratio between the output power to the motor P_{motor} and the electrical input power P_{elect} as

$$\eta_m = \frac{P_{motor}}{P_{elect}} \quad (12)$$

The electrical input power is calculated as the product of the supply voltage U_s and current i_s , which are measured by external sensors.

$$P_{elect} = U_s i_s \quad (13)$$

Therefore the ESC efficiency can be determined as

$$\eta_m = \frac{U_m i_m}{U_s i_s} \quad (14)$$

V. Validation Testing

The propulsion system testing apparatus underwent validation testing, confirming its ability to accurately measure performance and efficiency data under static and advancing flow conditions. The validation testing focused on verifying that the testing apparatus is able to correctly measure propeller thrust and torque as the mechanical design is new and untested. Calibration was also performed to verify cell output linearity. The electronic components of the propulsion system testing apparatus, including the ESC interface, airspeed sensor, supply voltmeter and ammeter, IMU, and GNSS receiver have already been used and validated elsewhere.⁴¹ Additionally, it is not expected that these electronic components require installation corrections.

A. Calibration

The propulsion system testing apparatus underwent thrust and torque calibration to verify linear output and determine the required calibration equations. Thrust calibration, shown in Fig. 6 (a), was performed using precision proof weights pulling a string around a low-friction pulley system to create an axial force, thereby simulating thrust being applied to the load cell. A total of 16 precision weights were added sequentially creating simulated load between 0 and 80% of the rated capacity. Torque calibration was performed with the 3D printed nose section removed and can be seen in Fig. 6 (b). A known moment arm was bolted to the torque load cell and precision weights were applied at a precisely measured location via a string. A total of 16 precision weights were added sequentially creating simulated torque between 0 and 88 % of the rated capacity. For both the thrust and torque calibrations, linear regression was performed on the data yielding R^2 values of greater than 0.995.

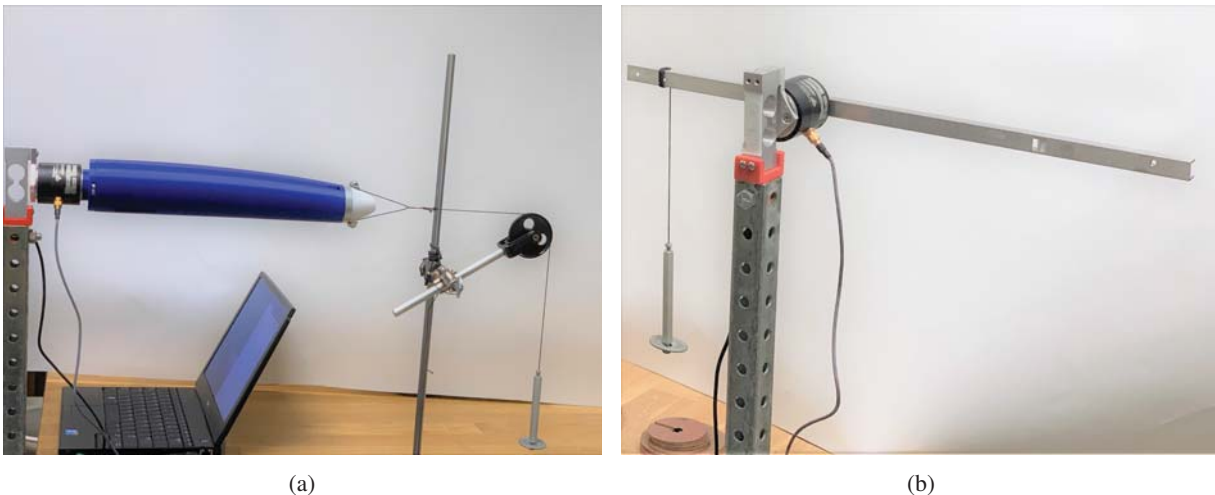


Figure 6: Calibration of the propulsion system testing apparatus: (a) thrust and (b) torque.

B. Static Testing

Static propeller testing was performed using several propellers with known performance curves for point of comparison. The propellers chosen were the APC 8×4 Thin Electric, APC 9×6 Sport, APC 10×5 Thin Electric, and APC 10×7 Thin Electric, which provided a range of diameters, pitch-to-diameter ratios, and geometries. These propellers were previously test by Brandt and Deters^{7,14} and the performance data are available on the UIUC Propeller Data Site.⁴²

Figures 7-10 show a comparison of the static run results for each of the propellers. The results for the APC 8×4 Thin Electric propeller show similarity in slope between the data sets, yet, there seems to be a constant offset. The results for the APC 9×6 Sport propeller are very similar for the thrust coefficient results, lying between the results of the two UIUC Propeller Data Site data sets. However, for the power coefficient results, there is some offset in the results. Specifically, there is also a notable difference between the two runs of the present work, within the 2500 to 4000 RPM range. Finally, the results for the APC 10×5 Thin Electric and APC 10×7 Thin Electric show very nice similarity between the UIUC Propeller Data Site data set and the present work data sets.

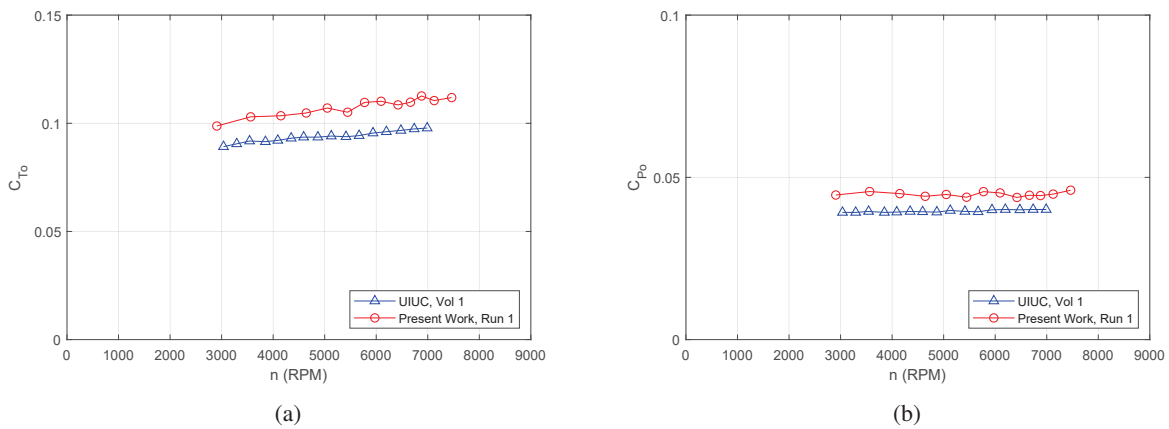


Figure 7: Comparison of static performance of the APC 8×4 Thin Electric propeller: (a) thrust coefficient and (b) power coefficient.

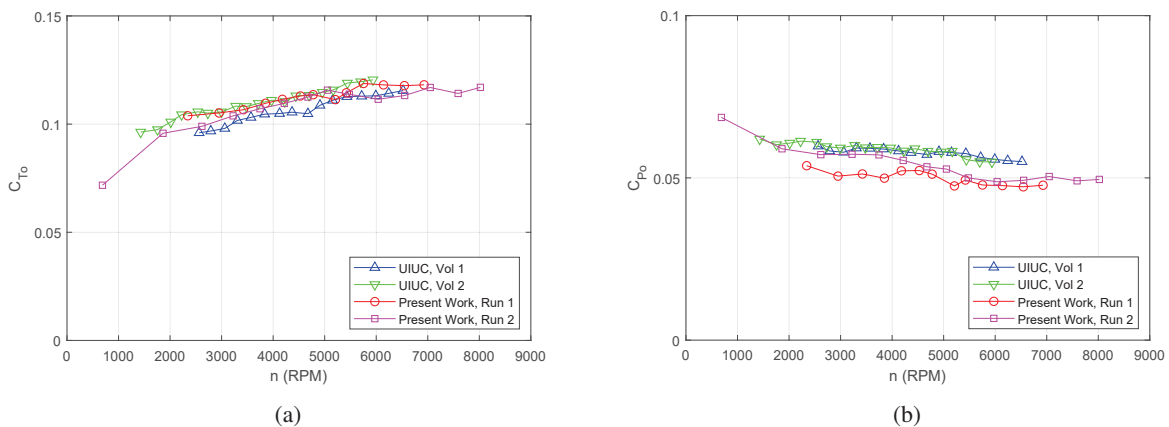


Figure 8: Comparison of static performance of the APC 9×6 Sport propeller: (a) thrust coefficient and (b) power coefficient.

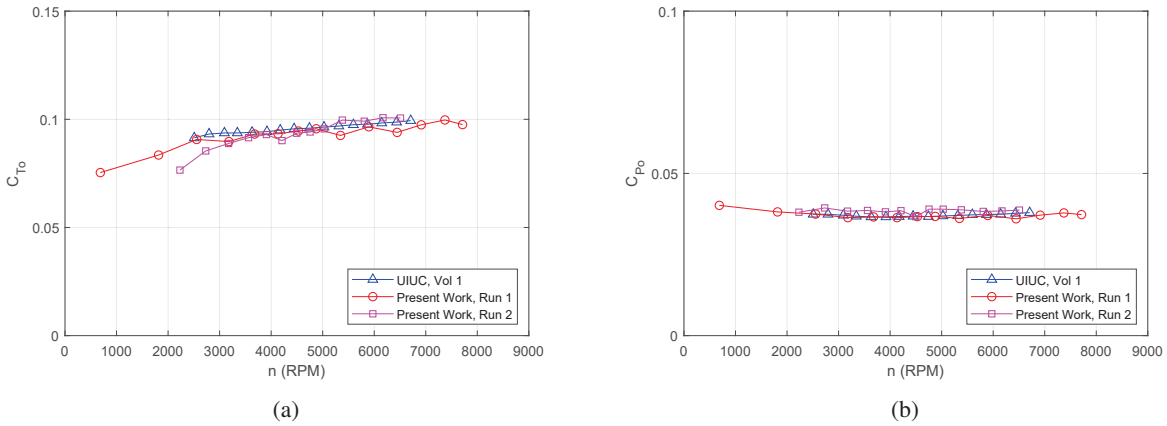


Figure 9: Comparison of static performance of the APC 10x5 Thin Electric propeller: (a) thrust coefficient and (b) power coefficient.

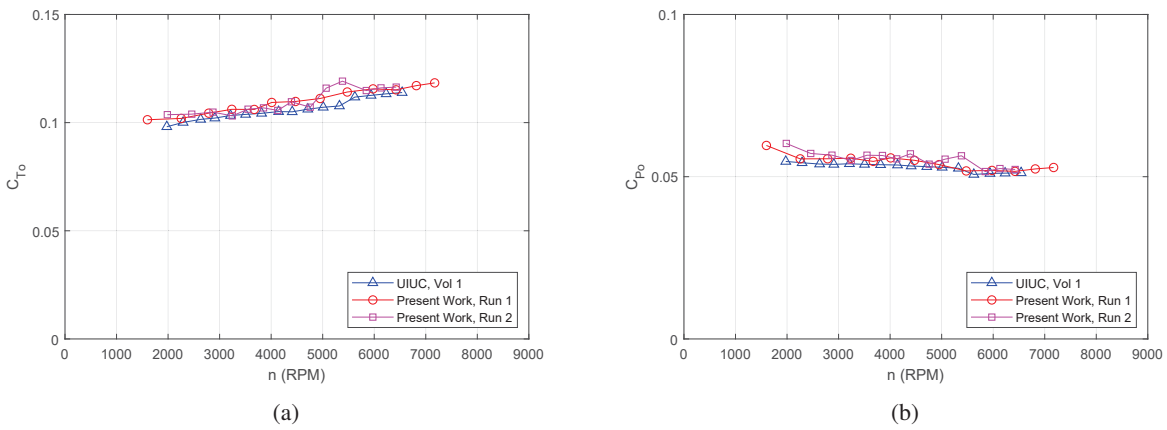


Figure 10: Comparison of static performance of the APC 10x7 Thin Electric propeller: (a) thrust coefficient and (b) power coefficient.

C. Advancing Flow Testing

Advancing flow testing was performed on the propulsion system testing apparatus using cartop testing; Fig. 11 shows the testing apparatus mounted a top the roof rack of a car. Two propellers were chosen for testing: APC 10x5 Thin Electric and APC 10x7 Thin Electric. The performance of these propellers was tested at by Brandt at UIUC and was later verified by testing by McCrink at OSU.⁴³

Figures 12 and 13 show a comparison of the advancing flow run results for each of the propellers. Each plot has three reference RPMs from the UIUC Propeller Data Site and three from the present work. There are two UIUC Propeller Data Site curves for each RPM, together providing a wide range of advance ratios; these curves are within 20 RPM of the stated values. The curves for the presented work are made up of samples within 50 RPM of the stated values. Overall there is reasonable correlation between the results. Reynolds number effects are visible for the UIUC Propeller Data Site data as well as for the results of the present work, especially for the APC 10x5 Thin Electric propeller. It is also believed that the outlier present would likely be discarded if additional samples were taken.



Figure 11: A photo of the propulsion system testing apparatus mounted atop a car for validation testing.

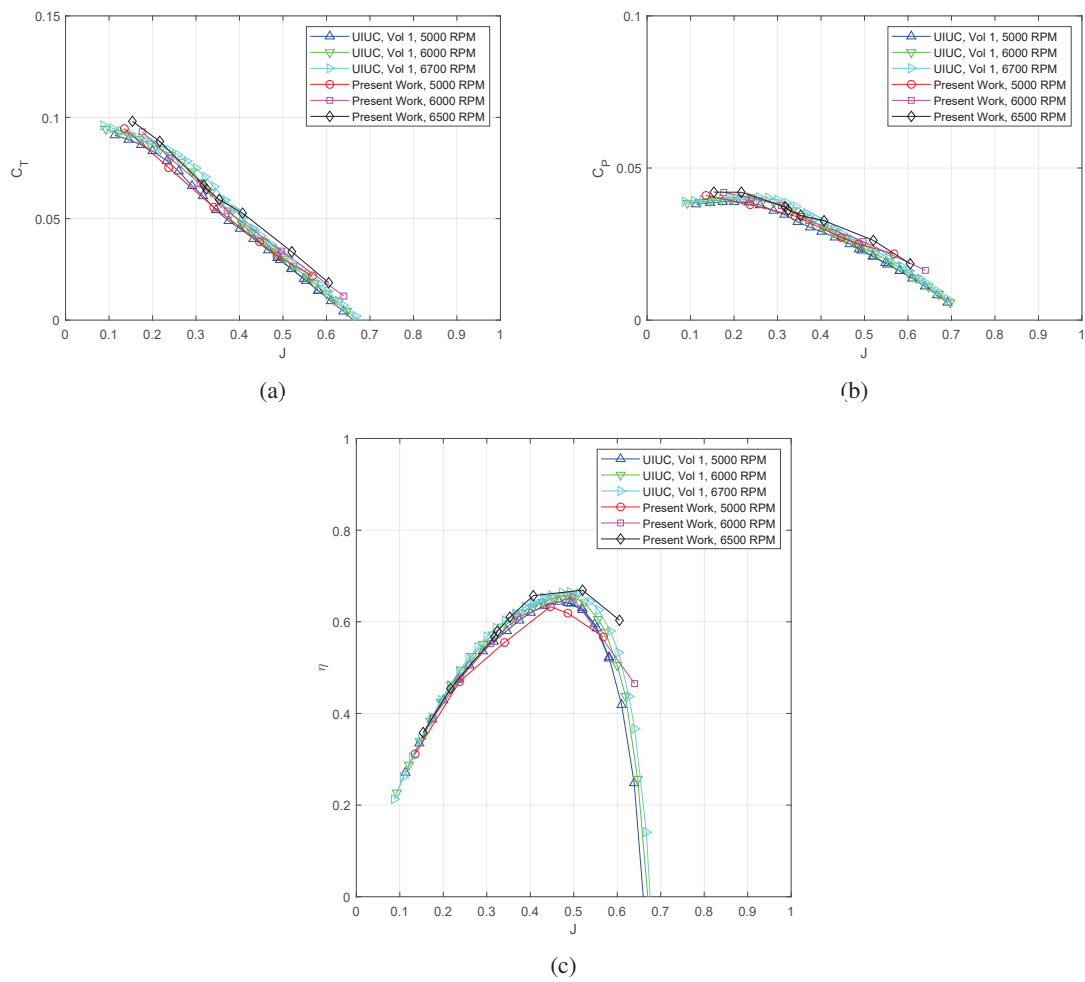


Figure 12: Comparison of advancing flow performance of the APC 10×5 Thin Electric propeller: (a) thrust coefficient, (b) power coefficient, (c) efficiency.

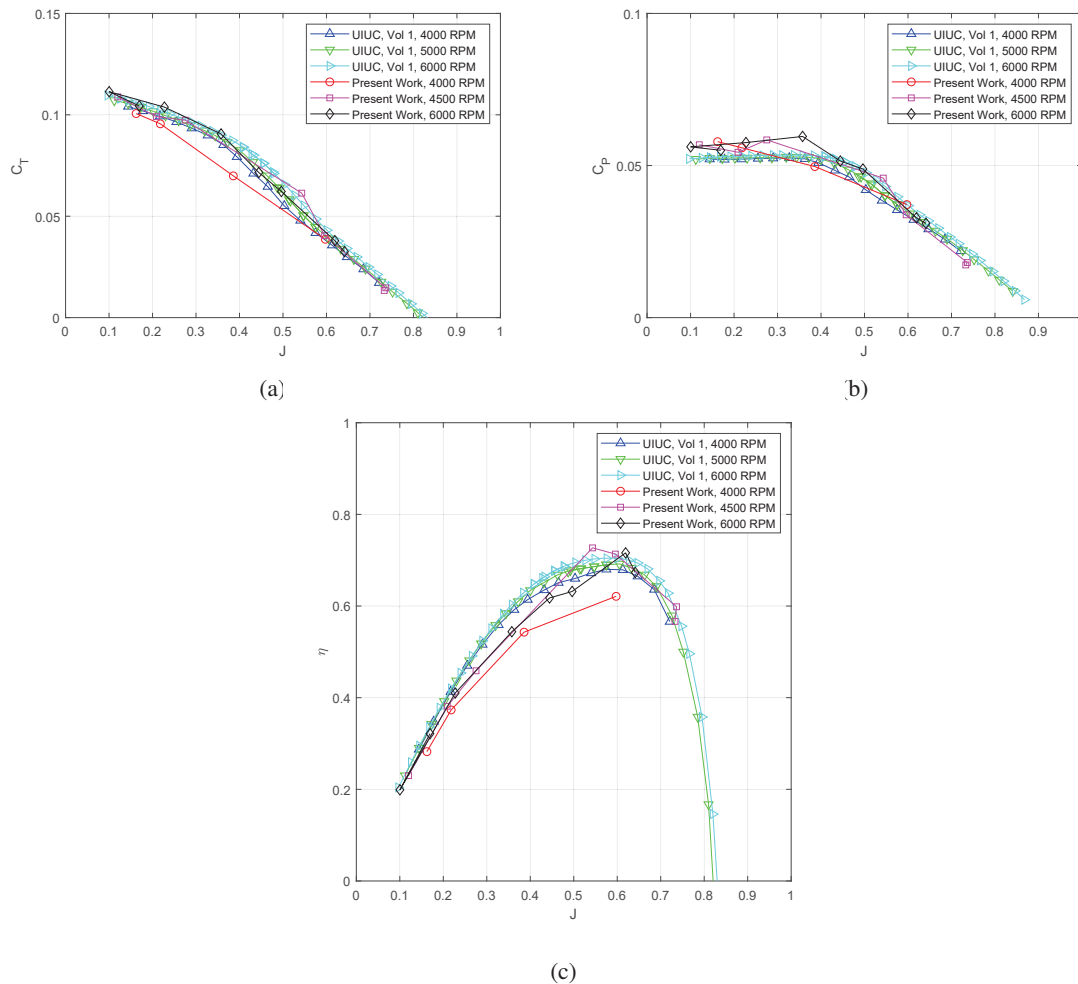


Figure 13: Comparison of advancing flow performance of the APC 10 \times 7 Thin Electric propeller: (a) thrust coefficient, (b) power coefficient, (c) efficiency.

VI. Summary and Future Work

This paper described the development and validation of a propulsion system testing apparatus that is designed to evaluate potential components for a long-endurance solar-powered unmanned aircraft. Specifically, the testing apparatus was developed to measure the performance and efficiency parameters of possible electric propulsion system components (propellers, motors, and ESC) while maintaining similar air flow characteristics, in either a wind tunnel or on a moving automotive platform. The propulsion system testing apparatus was instrumented with a high-frequency data acquisition system and sensors allowing for simultaneous load, torque, electrical, air data, and inertial measurement. The testing apparatus underwent calibration and validation testing, confirming its linearity and its ability to accurately measure performance and efficiency data under static and advancing flow conditions. Compared to existing works in the literature, the propulsion system testing apparatus presented in this paper allows for holistic testing of all possible compatible electric propulsion system components in a flight-like environment.

In future work, the propulsion system testing apparatus will be used to evaluate a variety of propeller and motors in order to complement the development of a solar-powered aircraft. Specifically, performance and efficiency testing of 31 propellers is planned as well as at least half a dozen motors. Currently, the propulsion system testing apparatus does not support the testing of the energy supply sources; however, the additional capability, to accommodate the testing of batteries, as well as other energy sources (e.g. solar arrays, fuel cells, or hybrid-electric), may be added in the near future.

Acknowledgments

The material presented in this paper is based upon work supported by the National Science Foundation (NSF) under grant number CNS-1646383. Marco Caccamo was also supported by an Alexander von Humboldt Professorship endowed by the German Federal Ministry of Education and Research. Any opinions, findings, and conclusions or recommendations expressed in this publication are those of the authors and do not necessarily reflect the views of the NSF.

The authors would like to thank AI Volo LLC for their generous loan of data acquisition equipment and Renato Mancuso for providing integration and testing support.

The authors would also like to acknowledge Bryce BeVier, Joseph Grigus, Saym Imtiaz, Derek Lai, Kyler Perez, and Moiz Vahora for their support during the development and testing.

References

- ¹“Altavian,” <http://www.altavian.com/>, Accessed May 2019.
- ²Precision Hawk, “Precision Agriculture, Commercial UAV and Farm Drones,” <http://precisionhawk.com/>, Accessed Apr. 2015.
- ³MicroPilot, “MicroPilot - MP-Vision,” <http://www.micropilot.com/products-mp-visione.htm>, Accessed Apr. 2015.
- ⁴Dantsker, O. D., Theile, M., and Caccamo, M., “Design, Development, and Initial Testing of a Computationally-Intensive, Long-Endurance Solar-Powered Unmanned Aircraft,” AIAA Paper 2018-4217, AIAA Applied Aerodynamics Conference, Atlanta, Georgia, June 2018.
- ⁵Real Time and Embedded System Laboratory, University of Illinois at Urbana-Champaign, “Solar-Powered Long-Endurance UAV for Real-Time Onboard Data Processing,” <http://rtsl-edge.cs.illinois.edu/UAV/>, Accessed Jan. 2018.
- ⁶Dantsker, O. D., Imtiaz, S., and Caccamo, M., “Electric Propulsion System Optimization for a Long-Endurance Solar-Powered Unmanned Aircraft,” Accepted to 2019 AIAA/IEEE Electric Aircraft Technologies Symposium, Indianapolis, Indiana, Aug. 2019.
- ⁷Brandt, J. B., *Small-Scale Propeller Performance at Low Speeds*, Master’s thesis, University of Illinois at Urbana-Champaign, Department of Aerospace Engineering, Urbana, IL, 2005.
- ⁸Bradt, J. B. and Selig, M. S., “Propeller Performance Data at Low Reynolds Numbers,” *AIAA Paper 2011-1255, AIAA Aerospace Sciences Meeting, Orlando, Florida, Jan. 2011*.
- ⁹Uhlig, D. V., *Post Stall Propeller Behavior at Low Reynolds Numbers*, Master’s thesis, University of Illinois at Urbana-Champaign, Department of Aerospace Engineering, Urbana, IL, 2007.
- ¹⁰Uhlig, D. V. and Selig, M. S., “Post Stall Propeller Behavior at Low Reynolds Numbers,” *AIAA Paper 2008-407, AIAA Aerospace Sciences Meeting, Reno, Nevada, Jan. 2008*.
- ¹¹Lundstrom, D., *Aircraft Design Automation and Subscale Testing*, Ph.D. thesis, Linkoping University, Department of Management and Engineering, Linkoping, Sweden, 2012.
- ¹²Lundstrom, D. and Krus, P., “Testing of Atmospheric Turbulence Effects on the Performance of Micro Air Vehicles,” *International Journal of Micro Air Vehicles*, Vol. 4, No. 2, Jun. 2012, pp. 133–149.
- ¹³Deters, R. W. and Selig, M. S., “Static Testing of Micro Propellers,” AIAA Paper 2008-6246, AIAA Applied Aerodynamics Conference, Honolulu, Hawaii, Aug. 2008.
- ¹⁴Deters, R. W., *Performance and Slipstream Characteristics of Small-Scale Propellers at Low Reynolds Numbers*, Ph.D. thesis, University of Illinois at Urbana-Champaign, Department of Aerospace Engineering, Urbana, IL, 2014.
- ¹⁵Deters, R. W., Kleinke, S., and Selig, M. S., “Static Testing of Propulsion Elements for Small Multirotor Unmanned Aerial Vehicles,” AIAA Paper 2017-3743, AIAA Aviation Forum, Denver, Colorado, June 2017.
- ¹⁶Deters, R. W., Dantsker, O. D., Kleinke, S., Norman, N., and Selig, M. S., “Static Performance Results of Propellers Used on Nano, Micro, and Mini Quadrotors,” AIAA Paper 2018-4122, AIAA Aviation Forum, Atlanta, Georgia, June 2018.
- ¹⁷Lindahl, P., Moog, E., and Shaw, S. R., “Simulation, Design, and Validation of an UAV SOFC Propulsion System,” *IEEE Transactions on Aerospace and Electronic Systems*, Vol. 48, No. 3, Jul. 2012, pp. 2582–2593.
- ¹⁸Chaney, C. S., Bahrami, J. K., Gavin, P. A., Shoemaker, E. D., Barrow, E. S., and Matveev, K. I., “Car-Top Test Module as a Low-Cost Alternative to Wind Tunnel Testing of UAV Propulsion Systems,” *Journal of Aerospace Engineering*, Vol. 27, No. 6, Nov. 2014.
- ¹⁹Dantsker, O. D., Selig, M. S., and Mancuso, R., “A Rolling Rig for Propeller Performance Testing,” AIAA Paper 2017-3745, AIAA Applied Aerodynamics Conference, Denver, Colorado, June 2017.
- ²⁰Drela, M., “DC Motor / Propeller Matching,” <http://web.mit.edu/drela/Public/web/qprop/motorprop.pdf>.
- ²¹Drela, M., “First-Order DC Electric Motor Model,” http://web.mit.edu/drela/Public/web/qprop/motor1_theory.pdf.
- ²²Drela, M., “Second-Order DC Electric Motor Model,” http://web.mit.edu/drela/Public/web/qprop/motor2_theory.pdf.
- ²³Green, C. R. and McDonald, R. A., “Modeling and Test of the Efficiency of Electronic Speed Controllers for Brushless DC Motors,” AIAA Paper 2015-3191, AIAA Aviation Forum, Dallas, Texas, Jun. 2015.
- ²⁴Gong, A. and Verstraete, D., “Experimental Testing of Electronic Speed Controllers for UAVs,” AIAA Paper 2017-4955, AIAA/SAE/ASCE Joint Propulsion Conference, Atlanta, Georgia, July 2017.
- ²⁵Gong, A., MacNeill, R., and Verstraete, D., “Performance Testing and Modeling of a Brushless DC Motor, Electronic Speed Controller and Propeller for a Small UAV,” AIAA Paper 2018-4584, AIAA Propulsion and Energy Forum, Cincinnati, Ohio, July 2018.

- ²⁶Gong, A., Maunder, H., and Verstraete, D., "Development of an in-flight thrust measurement system for UAVs," AIAA Paper 2017-5092, AIAA/SAE/ASEE Joint Propulsion Conference, Atlanta, Georgia, July 2017.
- ²⁷Mancuso, R., Dantsker, O. D., Caccamo, M., and Selig, M. S., "A Low-Power Architecture for High Frequency Sensor Acquisition in Many-DOF UAVs," Submitted to International Conference on Cyber-Physical Systems, Berlin, Germany, April 2014.
- ²⁸Dantsker, O. D., Mancuso, R., Selig, M. S., and Caccamo, M., "High-Frequency Sensor Data Acquisition System (SDAC) for Flight Control and Aerodynamic Data Collection Research on Small to Mid-Sized UAVs," AIAA Paper 2014-2565, AIAA Applied Aerodynamics Conference, Atlanta, Georgia, June 2014.
- ²⁹Dantsker, O. D. and Selig, M. S., "High Angle of Attack Flight of a Subscale Aerobatic Aircraft," AIAA Paper 2015-2568, AIAA Applied Aerodynamics Conference, Dallas, Texas, Jun. 2015.
- ³⁰Dantsker, O. D. and Mancuso, R., "Flight Data Acquisition Platform Development, Integration, and Operation on Small- to Medium-Sized Unmanned Aircraft," AIAA Paper 2019-1262, AIAA SciTech Forum, San Diego, California, Jan 2019.
- ³¹aero-naut Modellbau GmbH & Co. KG, "CAMcarbon folding propellers," <http://www.aero-naut.de/en/products/airplanes/accessories/propellers/camcarbon-folding-prop/>, Accessed Feb. 2018.
- ³²Corporation, L. M., "Stalker XE UAS," <https://www.lockheedmartin.com/en-us/products/stalker.html>, Accessed May. 2019.
- ³³Silent Falcon UAS Technologies, "Silent Falcon," <http://www.silentfalconuas.com/silent-falcon>, Accessed May. 2019.
- ³⁴Zipline International, "Zipline - Lifesaving Deliveries by Drone," <https://flyzipline.com/>, Accessed May. 2019.
- ³⁵Ltd., I. A. I., "Military Malat Products Bird Eye 400," http://www.iai.co.il/2013/36943-34720-en/Bird_Eye_Family.aspx, Accessed May. 2019.
- ³⁶Model Motors s.r.o., "AXI Model Motors," <http://www.modelmotors.cz/>, Accessed May 2019.
- ³⁷Hacker Motor GmbH, "Hacker Brushless Motors," <https://www.hacker-motor.com/>, Accessed May 2019.
- ³⁸Neutronics Inc., "NeuMotors," <https://neumotors.com/>, Accessed May 2019.
- ³⁹Al Volo LLC, "Al Volo: Flight Systems," <http://www.alvolo.us>.
- ⁴⁰Transducer Techniques LLC, "Load Cell - Load Cell Systems," <http://www.transducertechniques.com>.
- ⁴¹Dantsker, O. D., Theile, M., and Caccamo, M., "A High-Fidelity, Low-Order Propulsion Power Model for Fixed-Wing Electric Unmanned Aircraft," AIAA Paper 2018-5009, AIAA/IEEE Electric Aircraft Technologies Symposium, Cincinnati, OH, July 2018.
- ⁴²UIUC Applied Aerodynamics Group, "UIUC Propeller Data Site," <http://m-selig.ae.illinois.edu/props/propDB.html>.
- ⁴³McCrink, M. H. and Gregory, J. W., "Blade Element Momentum Modeling for Low-Re Small UAS Electric Propulsion Systems," AIAA Paper 2015-3191, AIAA Aviation Forum, Dallas, Texas, Jun. 2015.